# Monitoring morphology evolution within block copolymer microparticles during dispersion polymerisation in supercritical carbon dioxide: a high pressure SAXS study

*by* Tes Artikel Ji3

Polymer Chemistry

PAPER

View Article Online
View Journal | View Issue

Check for updates

Cite this: Polym. Chem., 2019, 10, 860

# Monitoring morphology evolution within block copolymer microparticles during dispersion polymerisation in supercritical carbon dioxide: a high pressure SAXS study†

Mohammad Alauhdin,‡[a] Thomas M. Bennett,‡[a] Guping He,[a] Simon P. Bassett,[a] Giuseppe Portale,[c] Wim Bras,[d] Daniel Hermida-Merino*[b] and Steven M. Howdle*[a]

Received 6th November 2018,
Accepted 21st December 2018

DOI: 10.1039/c8py01578c

rsc.li/polymers

Reversible addition–fragmentation chain transfer (RAFT) dispersion polymerisation in supercritical carbon dioxide is an effective process for creating block copolymer microparticles with internal nanostructures. Here we report an alternative synthesis route involving completely independent steps by exploiting the livingness of RAFT-terminated PMMA microparticles and their unique ability to be redispersed in $scCO_2$. This not only enables a series of block copolymers to be created from a single RAFT dispersion synthesised PMMA homopolymer batch, thus improving reproducibility, but also adds flexibility by allowing the time and concentration requirements for each stage to be decoupled. The internal morphology development and evolution for a series of poly(methyl methacrylate-*block*-styrene) (PMMA-*b*-PS) block copolymer microparticles synthesised *via* this route was monitored *via in situ* small-angle X-ray scattering (SAXS) using an autoclave with diamond windows. Together with offline kinetics experiments and post-mortem transmission electron microscopy imaging, this study provides remarkably detailed insights into block copolymer self-organisation phenomena in $scCO_2$. Specifically, the time period over which this block copolymer undergoes phase separation before progressing from an arrangement of spheres to lamellae *via* the hexagonal cylinder phase is elucidated, and the data are used to plot a detailed empirical phase diagram for this block copolymer system in $scCO_2$.

## Introduction

Block copolymers are a remarkable class of materials because of their ability to spontaneously self-organise into a variety of ordered mesoscopic morphologies. It is well understood that three parameters dictate this process: the volume fraction of each block ($f$), the Flory–Huggins polymer–polymer interaction parameter ($\chi$) and the degree of polymerisation ($N$).[1,2] For a linear A–B diblock copolymer the various morphologies that can be formed in this way include lamellae (LAM), cylinders (CYL), gyroids (GYR) and spheres (SPH), each of which can influence the physical properties of the overall material.[3–5] This has given rise to numerous studies aiming to exploit these structures for a diverse range of applications including drug delivery,[6] polyelectrolytes,[7,8] nanoporous membranes,[9] photonics,[10,11] thin film nanolithography,[12–14] organic photovoltaics[15] and as templates for inorganic materials.[16–18]

In more recent years the concept of confining self-assembled block copolymers within three dimensional micron-size structures such as spheres or worms has received considerable interest.[19] This is because the resulting hierarchically structured materials exhibit multiple levels of structural organisation simultaneously over disparate length scales, thus providing synergies between mechanical properties, transport properties and enhanced surface area.[20,21] A variety of novel approaches towards the synthesis of such materials have been actively investigated in the literature to date. The most common of these exploit solvent evaporation processes, typically from block copolymer solutions in solvent/nonsolvent mixtures such as the self-organised reprecipitation (SORP)[22–24] and evaporation-induced self-assembly (EISA)[25–27] methods, or dispersed

[a]School of Chemistry, The University of Nottingham, University Park, Nottingham, NG7 2RD, UK. E-mail: steve.howdle@nottingham.ac.uk
[b]Netherlands Organisation for Scientific Research (N.W.O), DUBBLE@ESRF, CS40220, 38043 Grenoble Cedex 9, France
[c]Zernike Institute for Advanced Materials, University of Groningen, Nijemborg 4, 9747 AG, The Netherlands
[d]Oak Ridge National Laboratory, Chemical Sciences Division, One Bethel Valley Road, Oak Ridge, Tennessee 37831, USA
†Electronic supplementary information (ESI) available. See DOI: 10.1039/c8py01578c
‡These authors contributed equally to this work.

in particles[28] or aerosols.[29] However, the drawbacks of these methods include the requirement for multiple steps, the use of volatile organic solvents and unrealistic reaction conditions (nano-object concentration typically <1 wt%) for scaled-up use.

An alternative route is the use of emulsion, miniemulsion or dispersion polymerisation, in which self-organisation occurs within a particle as the block copolymers are synthesised, typically using controlled/living radical polymerisation (CLRP) techniques. CLRP in dispersed systems can advantageously be prepared at high concentration or solid content (up to 40 wt%) and overall presents a simpler and potentially commercial route to block copolymer particles because the synthesis and self-organisation steps take place simultaneously.[19] RAFT polymerisation is one of the CLRP techniques that has received considerable attention in the preparation of functional block copolymers in this way.[30] In particular, RAFT dispersion polymerisation has been successfully applied in producing amphiphilic block copolymer nano-objects of controlled size and morphology through the robust and efficient polymerisation-induced self-assembly (PISA) route.[31–33] Recently, our group has reported a block copolymer synthesis route *via* RAFT dispersion polymerisation in supercritical carbon dioxide ($scCO_2$) which allowed the one-pot fabrication of unique nanostructured-block copolymer microparticles that would not normally be obtained in conventional media.[34–37]

Dispersion polymerisation in $scCO_2$ is an effective technique in this regard because $scCO_2$ is a good solvent for most common vinyl monomers and a non-solvent for their polymers. This process also allows the size and morphology of the resulting polymer particles to be readily tuned.[38] Moreover, $scCO_2$ as a polymerisation medium is not only beneficial as an alternative 'green' solvent, but also provides additional advantages such as simplified product recovery, lower processing temperature, and the absence of solvent residue.[39–42] These advantages arise from the ability of $scCO_2$ to swell and plasticise various polymers as a function of pressure.[39,43,44] This allows the block copolymers to self-organise during the polymerisation process, even at moderate temperatures, thereby circumventing the need for time consuming post polymerisation annealing and/or mixing steps. It has also been observed that blocking efficiencies obtained in $scCO_2$ are comparable with, and often favourable to, those observed in other CRP reactions in heterogeneous media. This was attributed to the high diffusivity of $scCO_2$ improving access of the second monomer to the polymerization *loci*.[35] However, one potential consequence of this phenomenon is a deviation of the internal morphology of the block copolymer systems investigated from that expected for a block copolymer of equivalent $f_A$ in the melt state. This has been attributed to changes in the apparent volume fraction of the segments in a $scCO_2$ environment due to variations in the $CO_2$-philicity of each block, thus altering and even inducing morphological transitions.[36,45,46] This effect was clearly evident after dissolving and solvent casting the as-synthesised block copolymer microparticles into bulk films, which after annealing returned to their predicted equilibrium morphologies.[34]

The phase separation behaviour of block copolymers is often studied using small angle X-ray scattering (SAXS) because it is a relatively non-destructive and high-throughput technique that can probe structural features on the nano-scale and also permits *in situ* measurements.[33,47–49] SAXS is commonly used in corroboration with other techniques, such as electron microscopy, because although it provides more representative information of the structural properties of a sample, the data can often be ambiguous when considering samples with unconventional and/or intermixed morphologies. A combination of transmission electron microscopy (TEM) and SAXS analysis has been utilised previously to fully characterise the microphase separation within block copolymer microparticles prepared in $scCO_2$ and confirm the persistence of the observed morphology throughout an entire sample.[34,36] Recently, synchrotron radiation SAXS studies were undertaken for the first time to investigate the morphological transitions that occur *in situ* during the non-aqueous PISA synthesis of poly(stearyl methacrylate)-*b*-poly(benzyl methacrylate) (PSMA-*b*-PBzMA) diblock copolymers.[50] An *in situ* SAXS kinetics study has also demonstrated that morphology changes during the synthesis of a PMMA-*b*-PBzMA block copolymer microparticle sample *via* RAFT dispersion polymerisation in $scCO_2$ could be detected, but no interpretation of the order development and thermodynamics of the system were discussed.[51]

Given that many of the desirable properties of block copolymers originate from their well-defined nanostructures, the ability to precisely predict when an ordered morphology will form and what structure it will take are crucial pieces of information. This article describes several advances in the synthesis of block copolymer microparticles *via* dispersion polymerisation in $scCO_2$ and the characterisation of their internal structures. Most importantly, we demonstrate that the synthesis of nanostructured block copolymer microparticles can be separated into two completely independent steps. We exploit the livingness of RAFT-terminated macro chain transfer agent (macroCTA) PMMA microparticles, which retain activity even after storage for several months, and their ability to be redispersed in $scCO_2$. This enables a series of block copolymers to be created from a single RAFT dispersion synthesised PMMA homopolymer batch, thus improving reproducibility and also increasing flexibility by allowing the time and concentration requirements for each stage to be decoupled. We then monitored the internal morphology development and subsequent evolution for a series of PMMA-*b*-PS block copolymer microparticles synthesised using this route *via in situ* SAXS. Together with offline kinetics experiments and TEM characterisation this approach provides remarkably detailed insights of the self-organisation process occurring within block copolymer microparticles in $scCO_2$.

## Experimental

### Materials

*S*-Dodecyl-*S*′-(α,α′-dimethyl-α″-acetic acid) trithiocarbonate (DATC) was synthesised following literature procedures.[52]

α-Azobisisobutyronitrile (AIBN, Wako, 97%) was purified by recrystallising twice from methanol. Methyl methacrylate (MMA, Fisher, >99%) and styrene (Alfa Aesar, 99%) were purified by eluting through a column of basic alumina prior to use. Poly(dimethylsiloxane monomethyl methacrylate) (PDMS-MA, ABCR, number-average molecular weight ($M_n$) = 10 000 g mol$^{-1}$) and ruthenium tetroxide ($RuO_4$, Acros, 0.5% solution in water) was used as received. Dry $CO_2$ (SFC grade, 99.99%) was purchased from BOC or Air Liquide. HPLC grade THF (Fisher) and HPLC grade chloroform (Aldrich) were used without further purification. For TEM, Agar 100 epoxy resin (Agar Scientific) was used as received, and mixed to target a formulation of medium hardness for embedding samples before being allowed to set at 50 °C for 48 hours.

### RAFT dispersion polymerisation of MMA in $scCO_2$

The RAFT dispersion polymerisation of PMMA has been reported previously.[53] In a typical procedure targeting PMMA with a molecular weight of 25 kDa, RAFT agent (DATC, 165 mg, 0.45 mmol), AIBN (73 mg, 0.23 mmol) and macromonomer stabiliser (PDMS-MA, 5 wt% relative to MMA) were added to a standard 60 mL autoclave. The autoclave was purged with $CO_2$ for 30 minutes, during which time MMA (11.3 g, 112.7 mmol) was degassed by bubbling with argon at 0 °C before being charged into the autoclave under a positive flow of $CO_2$. The autoclave was then sealed and pressurised to 50 bar, heated to 65 °C and then the pressure was topped up to 275 bar. The reaction was stirred at 300 rpm for 18 hours, after which time the heating jacket was switched off and the autoclave was vented over a period of 15 minutes upon cooling to ambient temperature. In all cases the PMMA product was collected as a fine, pale yellow powder with gravimetric conversions >95%.

### X-ray autoclave characteristics

An improved version of the X-ray autoclave previously developed by the Howdle group[51] was constructed in-house at the University of Nottingham and used for all of the SAXS monitored reactions (see ESI Fig. S1†). The features of this design are a 60 mL capacity and working pressure and temperature limits of 300 bar and 120 °C, respectively. In addition, the X-ray windows are mounted in a small, independent holder that facilitates efficient stirring throughout the vessel, crucial for *in situ* polymerisation studies, and also aids product collection and cleaning when removed post reaction.

### Small-angle X-ray scattering setup

Time-resolved SAXS experiments were conducted at the Dutch-Belgian Beamline (DUBBLE) station BM26-B of the European Synchrotron and Radiation Facility (ESRF) in Grenoble, France.[54] Experiments were performed using a wavelength ($\lambda$) of 0.6526 Å (15 KeV) and a sample-to-detector distance of 3000 m. A Dectris-Pilatus 1 M detector with a resolution of 981 × 1043 pixels and a pixel size of 172 × 172 μm was employed to record the 2D scattering profiles, covering a scattering angle range $q$ = 0.07–3.65 nm$^{-1}$, where the modulus of the scattering vector $q$ is defined as $q = 4\pi/\lambda \sin\theta$, with $2\theta$ being the scattering angle. SAXS profiles of the reaction mixtures were collected every 2.5 minutes, with an exposure time of 30 seconds. The diffraction rings from a Silver Behenate powder standard were used to calibrate the scattering angle scale. The SAXS images were normalised with respect to the incident beam intensity and were corrected for absorption and background scattering from the diamond windows and $scCO_2$ within the autoclave. After correction, radial averaging around the beam centre was conducted in order to covert the SAXS images into the $I(q)$ *vs.* $q$ curves.

### Chain extension of PMMA microparticles with styrene monitored *via in situ* small-angle X-ray scattering in $scCO_2$

The polymers described here are designated with the generalized label PMMA($X$) and PS($X$), where $X$ denotes the $M_n$ values in kDa. In a typical reaction, the chain extension of PMMA(31) with PS(25) was monitored *in situ via* time resolved SAXS. MacroCTA PMMA microparticles (5.94 g, 0.192 mmol), synthesised as described above, were added to the X-ray autoclave along with the PDMS-MA (5 wt% relative to styrene monomer) stabiliser. After gently purging the X-ray autoclave with $CO_2$ for 30 minutes, the vessel was sealed, pressurised to 50 bar and then heated to 65 °C before finally topping up the pressure to 275 bar. After stirring for at least 2 hours at 300 rpm under these conditions, the pressure inside the X-ray autoclave was reduced to 200 bar and styrene (5.45 g, 52.3 mmol) containing AIBN (30 mg, 0.093 mmol), which had been degassed by bubbling with argon for 30 minutes, was injected through the head of the autoclave at a rate of 1 mL min$^{-1}$ using a HPLC pump (Jasco). The styrene was allowed to polymerise for 64 hours, during which time SAXS profiles of the reaction mixture were collected every 2.5 minutes with an exposure time of 30 seconds. On completion, the temperature was reduced to ambient over a period of approximately 1 hour, and the X-ray autoclave was vented over an additional period of approximately 4 minutes. In each case involving styrene monomer the products were collected as pale yellow and slightly clumped powders due to microparticle surface dissolution and partial fusion by the residual monomer. For the reaction involving the synthesis of PMMA-*b*-PMMA a homogeneous fine pale yellow powder was obtained instead.

### Offline kinetics investigation of the chain extension of macroCTA PMMA microparticles with styrene *via* reaction sampling

The representative chain extension of PMMA(25) (3.34 g, 0.134 mmol) with styrene (10 g, 96.0 mmol) was repeated offline in a 60 mL stainless steel autoclave with a sampling tap on the base to collect the polymer product at various times throughout the polymerisation. This was performed as described above for the *in situ* experiments using AIBN (25 mg, 0.077 mmol), with the exception that at time periods of 21, 37, 53, 60 and 84 hours, a ~1 mL closed sampling pipe was screwed onto the bottom of the reactor and the sampling tap was opened to the reaction for 5 seconds.

### Polymer characterisation

PMMA-*b*-PS block copolymers were analysed by $^1$H NMR in $CDCl_3$ on a Bruker DPX 400 MHz spectrometer in order to determine the molecular weight of the polystyrene blocks ($M_n$, $^1$H NMR) and the overall mass fraction of the block copolymers. This was converted to the PMMA volume fraction ($f_{PMMA}$) using the reported mass densities of the individual homopolymers: PMMA = 1.17 g cm$^{-3}$ and PS = 1.05 g cm$^{-3}$.[55] The molecular weight ($M_n$, GPC) and the dispersity ($Đ$) of the homo and block copolymers were also determined by GPC using either an Agilent PL GPC 120 in THF or a PL GPC 50 in chloroform. Analyses were run at 40 °C with flow rates of 1 mL min$^{-1}$ and 0.5 mL min$^{-1}$, respectively, and the columns were calibrated with narrow dispersity PMMA standards.

### Transmission electron microscopy (TEM)

Block copolymer particles were embedded in epoxy resin (Agar 100) and set at 50 °C for 48 hours before being ultramicrotomed at room temperature to ~100 nm slices with a diamond knife (Leica Diatome Ultra 45°) and collected on copper grids. Where specified, the PMMA-*b*-PS particle sections were stained prior to imaging with $RuO_4$ for 2 hours, which adsorbs selectively to PS. Imaging of particle samples was completed using a FEI Tecnai TEM operating at an accelerating voltage of 100 kV.

## Results and discussion

### Synthesis and characterisation of PMMA microparticles in scCO$_2$

In previous publications we reported on the one pot RAFT dispersion synthesis of structured block copolymer microparticles in scCO$_2$. In this scenario the second monomer was injected under pressure once the MMA polymerisation had reached high conversion.[35,36] Here we explore a much improved "two-pot" route that separates the block copolymer synthesis into two independent pressurisation/polymerisation/depressurisation stages. The success of this approach hinges on retaining the "livingness" of the PMMA seed particles and successfully redispersing them in scCO$_2$ prior to adding the second monomer. Such redispersion can be achieved by incorporating additional PDMS-MA stabiliser into the vessel to account for the volume increase of the particles as $M_n$ increases, allowing a series of previously synthesised PMMA particles to be chain extended.[53] The role of the additional PDMS-MA stabiliser in improving the redispersion process was determined through a series of test polymerisations undertaken prior to the reactions described here. In these cases, chain extension of the macroCTA PMMA microparticles was still observed, but the block copolymer microparticle products were very poorly defined (ESI Fig. S2†).

In the first stage of the process, a series of PMMA microparticle batches with varying $M_n$ values (Table 1) were synthesised *via* RAFT dispersion polymerisation in scCO$_2$, and then used for chain extension experiments monitored *via in situ* SAXS

**Table 1** Characteristics of the PMMA particles prepared *via* dispersion polymerisation in scCO$_2$

| Exp. | Name | $M_{n,\,theo.}$[a] (kDa) | $M_{n,\,exp.}$[b] (kDa) | $Đ$[b] | Conv.[c] (%) |
|---|---|---|---|---|---|
| 1 | PMMA(31) | 30 | 31 | 1.16 | 96 |
| 2 | PMMA(25) | 25 | 25 | 1.19 | 95 |
| 3 | PMMA(58) | 50 | 58 | 1.39 | 98 |
| 4 | PMMA(54) | 50 | 54 | 1.19 | 98 |

[a] $M_{n,theo}$ was calculated by: [MMA]/[RAFT] × 100.11. [b] Determined by GPC in THF against PMMA standards. [c] Determined gravimetrically.

(Scheme 1a).[53] In each case excellent molecular weight control and narrow dispersity values were achieved as confirmed by the GPC traces (ESI Fig. S3†), demonstrating that the DATC RAFT agent in the seed particles was active and able to control the polymerisations effectively. Analysis of each product with SEM revealed that discrete spherical particles were formed in all cases with sizes ranging between 1.7–2.2 μm (ESI Fig. S4†).

### PMMA microparticle chain extensions in scCO$_2$ monitored *via in situ* SAXS

Four different chain extension reactions were monitored *via* time-resolved SAXS *in situ*. The characteristics of the final products (GPC, $^1$H NMR, DSC and TEM analysis of the morphology) are listed in Table 2 (see ESI Fig. S3 and S5† for the GPC and DSC traces for each sample, respectively). Here the experiment numbers 5–8 correspond respectively with chain extension reactions of PMMA homopolymers 1–4 (Table 1). Styrene was selected as the second monomer because (a) PMMA and PS domains have high X-ray contrast, (b) the Flory–Huggins polymer–polymer interaction parameter ($\chi$) of this diblock copolymer is known,[56] and (c) the phase behaviour has been widely investigated both in the bulk[12,57] and solution states,[58,59] including in scCO$_2$.[34] Furthermore, PMMA and PS have considerably different CO$_2$-affinities,[60] and the small $k_p$ for styrene means the polymerisation proceeds over a greater time period,[61] allowing subtle or slow changes in the phase behaviour due to molecular weight or scCO$_2$ swelling to be tracked and potentially decoupled more effectively using the SAXS profiles.

For each polymerisation, a constant PMMA loading of 5 grams was used along with 5 wt% of PDMS-MA stabiliser, which were stirred together at the reaction temperature and pressure (65 °C and 275 bar) for a minimum of 2 hours in order to redisperse the microparticles prior to adding the styrene monomer (Scheme 1b). The styrene polymerization kinetics were studied for experiments 5 and 6 in a standard 60 mL sampling autoclave, as described further in the ESI (see also ESI Fig. S6 and S7†). These reactions revealed that the styrene polymerisation ultimately takes >72 hours to reach high conversion (>90%), meaning that achieving full conversion at the beamline was not possible in the time frame available. This explains the discrepancy between the targeted and obtained $M_n$ values for each polymer synthesized during *in situ*

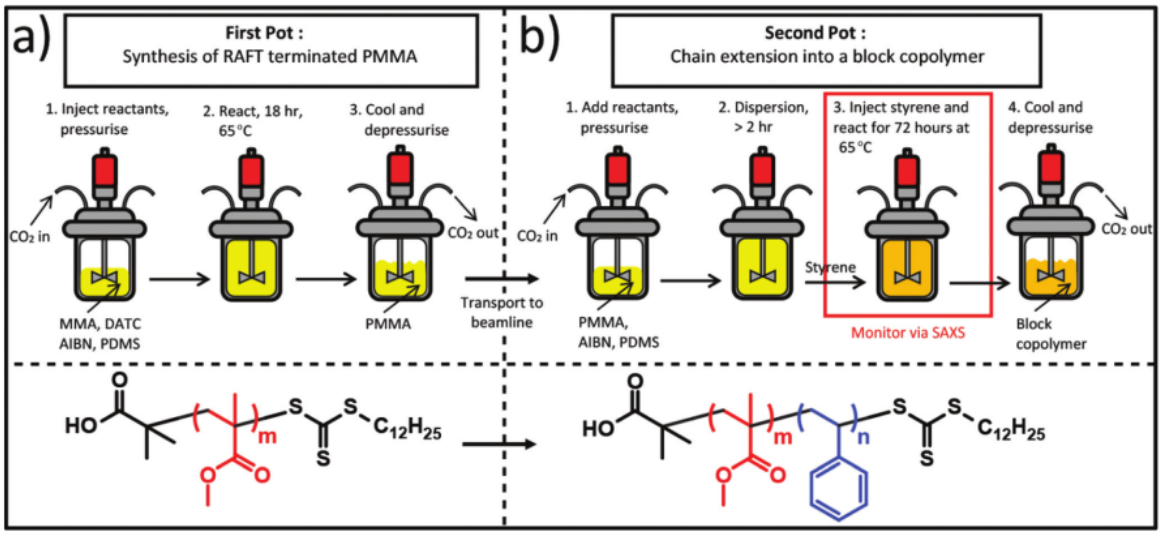


**Scheme 1** The "two pot" synthesis method used to prepare the block copolymers monitored *via* time resolved SAXS. (a) Preparation of PMMA particles *via* dispersion polymerisation and (b) PMMA particle redispersion with additional PDMS-MA stabiliser and subsequent chain extension with styrene at the beamline.

**Table 2** Characteristics of the PMMA-*b*-PS products synthesised during the *in situ* SAXS characterisation

| Exp. | Name | Block 2 reaction time (h) | $M_n$ theo (BCP, kDa)[a] | $M_n$ exp. (BCP, kDa)[c] | $f_{PMMA}$[c] | $Đ$[b] | Morph.[d] | $T_{g,PMMA}$[e] (°C) | $T_{g,PS}$[e] (°C) | Conv.[f] (%) |
|---|---|---|---|---|---|---|---|---|---|---|
| 5 | PMMA(31)-PS(25) | 64 | 70 | 55.7 | 0.53 | 1.5 | CYL | 118.4 | 95.5 | 79 |
| 6 | PMMA(25)-PS(50) | 63 | 100 | 75 | 0.31 | 1.84 | CYL/LAM | 118.2 | 95.1 | 80 |
| 7 | PMMA(58)-PS(12) | 71 | 80 | 70.2 | 0.81 | 1.51 | DIS | 122.5 | N/O | 76 |
| 8 | PMMA(54)-PMMA(44) | 23 | 100 | 95.4 | 1.00 | 1.45 | DIS | 123.0 | N/A | 97 |

[a] $M_{n,theo}$ was calculated by: [Monomer]/[PMMA macroCTA] × MW monomer. [b] Determined by GPC in THF against PMMA standards. [c] From $^1$H NMR. [d] From TEM images. [e] Measured by DSC, N/O = not observed due to a lack of phase separation. [f] Determined gravimetrically, residual monomer present.

SAXS monitoring (Table 2). We also note here that the molar mass dispersity values for the block copolymers synthesised here are typically higher than for analogous homogeneous solution based syntheses. However, these values are comparable to results reported previously for this block copolymer system by our group using the one-pot approach,[35] as well as other examples of heterogeneous syntheses in the literature. This is attributed to the higher tendency of styrenic monomers to terminate by combination, particularly under monomer starved conditions, as is the case in the latter stages of the polymerisations reactions undertaken here.[62] In order to understand the influence of block copolymer composition on order development and phase transitions in these systems, the molecular weights of the PS blocks across the three polymerisations were targeted to obtain block ratios in the final products of $f_{PMMA} \approx f_{PS}$ (experiment 5), $f_{PMMA} \ll f_{PS}$ (experiment 6) and $f_{PMMA} \gg f_{PS}$ (experiment 7). A control experiment in which PMMA was chain extended with a second PMMA block of comparable $M_n$ was also completed (experiment 8).

### Internal morphology development and evolution during the polymerisation of PMMA(31)-PS(25)

Time-resolved SAXS profiles were recorded during the chain extension of PMMA(31) to PMMA(31)-PS(25) and plotted as a 3-dimensional $q$ (nm$^{-1}$) *versus* intensity ($I(q)$) *versus* time ($t$) plot to illustrate the morphological transitions throughout the polymerisation (Fig. 1). A large number of SAXS profiles were removed to improve the overall visibility of the data, with the remaining profiles being separated by approximately 30 minutes intervals. A second 2-dimensional plot of the data at 10 hours intervals was also created to further highlight the changes in the scattering patterns that occurred throughout the duration of the polymerisation (ESI Fig. S8†). The small gaps in the data are due to brief pauses during the data acquisition to either adjust the pressure or due to beam loss. The SAXS profiles are initially featureless and exhibit Porod scattering with $I(q) \propto q^{-4}$, indicating the presence of many large structures with sharp interfaces between them that are consist-

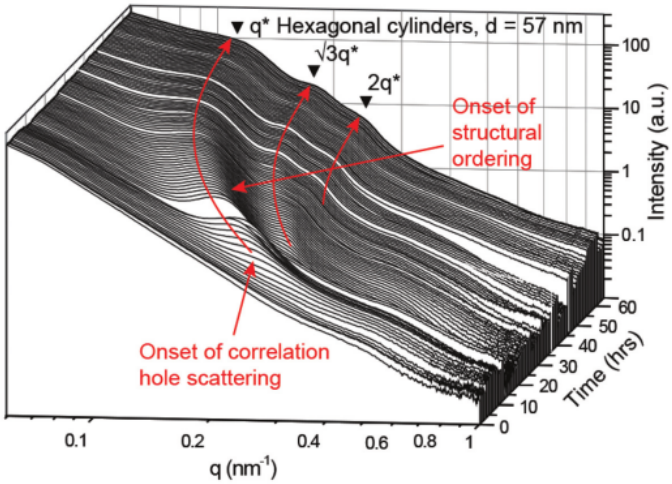


**Fig. 1** Time-resolved *in situ* SAXS data collected during the chain extension of PMMA(31) to form PMMA(31)-PS(25) (experiment 5) *via* dispersion polymerisation in $scCO_2$. The time between the individual profiles included is approximately 30 minutes.

ent with the overall size of the polymer microparticles without any internal nanostructure.[63] This is highlighted in the ESI,† where the SAXS profile for the sample taken at $t = 0$ is plotted alongside the $q^{-4}$ decay data (ESI Fig. S9†). After polymerising for approximately 6 hours the first evidence of the formation of a block copolymer disordered phase is distinguishable by the formation of a very broad primary scattering ($q^*$) peak centred at 0.232 $nm^{-1}$ due to correlation hole scattering between the PMMA and PS segments enforced by their connectivity (Fig. 1, $q^*$) (see ESI eqn (S1)† for the peak fitting function used to derive the peak positions).[1,64]

The intensity of this peak then continues to increase over the next 10 hours and it simultaneously becomes narrower, as expected for a system that is progressing towards a more ordered state (Fig. 1). After 16 hours the block copolymer undergoes a disorder-to-order transition (DOT) as evidenced by the appearance of an additional higher order scattering peak centred at $\sqrt{3}q^*$ (Fig. 1, $\sqrt{3}q^*$). A secondary peak in this position is characteristic of a hexagonally packed cylindrical morphology, an assignment that was further validated by the appearance of a third characteristic peak for this morphology centred at $\sqrt{4} = 2q^*$ after approximately 30 hours (Fig. 1, $2q^*$). The intensity of these three SAXS peaks continues to increase throughout the remainder of the polymerisation and the domain spacing of the cylindrical morphology also continues to grow at a steady rate, culminating in a $q^*$ peak at 0.110 $nm^{-1}$. This corresponds with an average characteristic spacing of the cylindrical BCP morphology ($d_{CYL}$) in $scCO_2$ of 57.1 nm, as determined using Bragg's law:

$$d = 2\pi/q^* \quad (1)$$

The increase of $d_{CYL}$ during the PS polymerization indicates that the value of $\chi N$ for the system increased continuously until the time when the reaction was discontinued, in agreement with our kinetic studies (ESI Fig. S6 and S7†). We also note that the SAXS maxima throughout the course of the reaction remain relatively broad. This phenomenon has been previously reported in SAXS studies on these systems and suggests that the internal morphology is composed of a distribution of domain sizes that only persist over a relatively short range order, given that the peak width is inversely proportional to the degree of ordering.[36]

TEM images were acquired from thin sections of the final polymer product to corroborate the hexagonally packed cylinder internal morphology of the microparticles indicated by the SAXS profiles toward the end of the reaction (Fig. 2). These images verify the occurrence of this morphology, in agreement with previous studies on this block copolymer system with comparable values of $f_{PMMA}$.[34,36] Domain size measurements taken from the TEM images returned a value of approximately 44.2 nm from 50 measurements (cylinder-to-cylinder distance of $(2/\sqrt{3}) \times 44.2$ nm = 51.0 nm), but some variation in the domain size throughout each particle was observed, as expected from the broad nature of the reflections in the SAXS data. Nevertheless, this average value is slightly smaller than the 57.1 nm domain size calculated from the primary scattering peak in the final SAXS profile for the sample prior to depressurisation. To confirm whether the TEM measured value was representative of the sample as a whole or an artefact of the microtoming process, a post reaction SAXS profile was recorded after the final product had been collected (ESI Fig. S10†). This profile returned a value of 53.3 nm that was more comparable to that obtained prior to venting the $CO_2$, suggesting the discrepancy between the SAXS and TEM domain size measurements is most likely the result of sample distortion during the microtoming process, which can be difficult to avoid.[34]

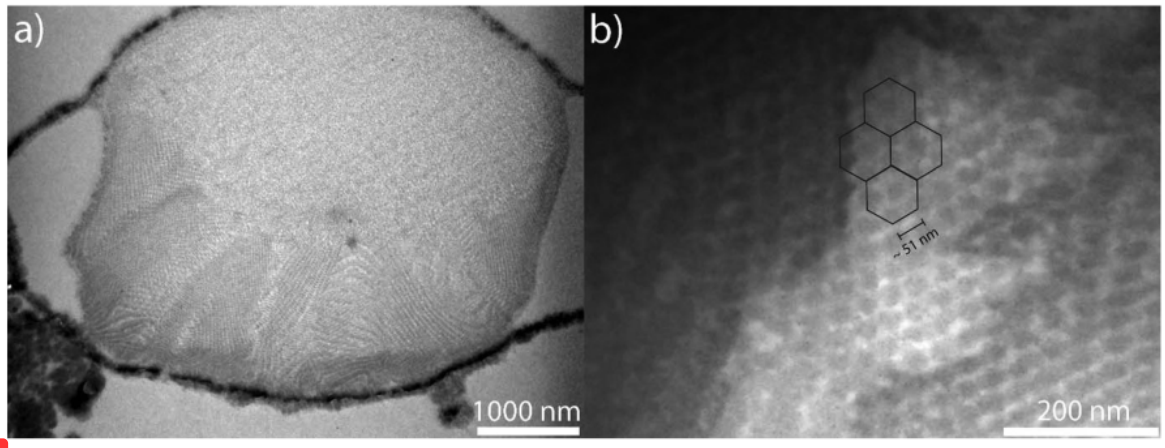


Fig. 2 (a) TEM images of a representative cross-sectioned PMMA-b-PS particle obtained following the chain extension of PMMA(31) with PS(25) in the X-ray autoclave. (b) A hexagonally packed cylinder morphology can be observed throughout the sample with a cylinder-to-cylinder distance of ~51 nm. The PS domains appear dark in both images due to staining with $RuO_4$.

### Internal morphology development and evolution during the polymerisation of PMMA(25)-PS(50)

A three dimensional $q$ ($nm^{-1}$) *versus* $I(q)$ *versus* $t$ plot was generated from the SAXS data obtained during the chain extension of PMMA(25) with PS(50), with a large number of SAXS profiles again being removed to improve the overall visibility of the data (Fig. 3a). A second 2-dimensional plot of the data at 10 hours intervals was also created to further highlight the changes in the scattering patterns that occurred throughout the duration of the polymerisation (ESI Fig. S11†). As was observed for PMMA(31)-PS(25), the SAXS profiles near the beginning of the reaction exhibit the characteristic Porod scattering of a microparticulate sample without internal structure. After 13.5 hours of PS polymerization, a broad and low intensity peak at around 0.22 $nm^{-1}$ appears and continues to develop over the next 10–15 hours (Fig. 3). As in the previous case, this peak is due to correlation hole scattering between the PMMA and PS segments, not able to show ordering due to the low $\chi N$ value at this point of the reaction. As the polymerization reaction progresses this peak gradually becomes more intense, forming a broad correlation peak that extends from 0.140–0.185 $nm^{-1}$ (Fig. 3a). This broad peak shows similarities with correlation peaks usually observed in systems comprised of interacting but poorly ordered spherical objects.[50] Thus, at the early stages of the reaction (before 30 hours) it appears

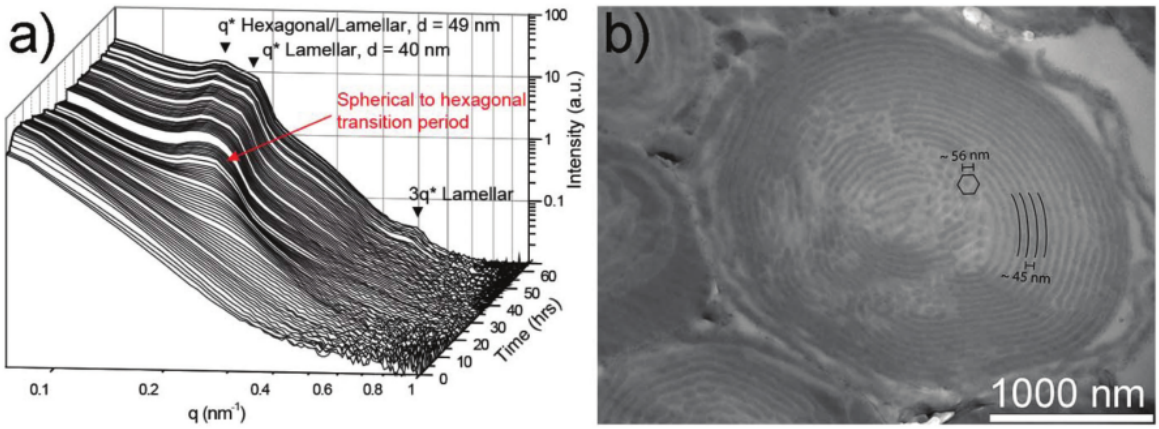


Fig. 3 (a) Time-resolved *in situ* SAXS profiles collected throughout the dispersion polymerisation of PMMA(25)-PS(50) in $scCO_2$. (b) TEM images of representative cross-sectioned PMMA(25)-PS(50) microparticles synthesised in the X-ray autoclave and collected at the end of the reaction. The majority of microparticles exhibit a coexisting mix of both morphologies, with lamellar being predominant towards the particle exterior. The PS domains appear dark due to staining with $RuO_4$. The time between the individual profiles included is approximately 30 minutes.

 

that spherical PS domains were beginning to form within the PMMA microparticles.

Over time this peak then continuously shifts towards lower $q$-values, again indicating that the molecular weight of the polystyrene block was gradually increasing. From approximatley 35 hours onwards this peak then gradually begins to separate into two distinct maxima at 0.0167 $nm^{-1}$ and 0.0194 $nm^{-1}$. This is indicative of a morphology transition within the sample, the specific nature of which cannot be assigned from this information alone. Finally, a third reflection with a much higher $q$ value in the range of 0.48 $nm^{-1}$ also becomes apparent from approximately 50 hours onwards (Fig. 3a, $3q^*$). A peak in this range is expected to be a higher order scattering reflection that suggests the sample has progressed to a more ordered state in which the domain spacing and/or morphology is more consistent throughout the microparticles. An offline SAXS profile was also recorded for the final product upon venting the autoclave, confirming almost no change in the domain size of these samples after removing the $scCO_2$, as for experiment 5 above (ESI Fig. S12†).

TEM images were taken from ~100 nm thick sections of the final product to validate the morphological transitions throughout the polymerisation (Fig. 3b). Intriguingly, the majority of the microparticles exhibit internal morphologies in which the lamellar phase is predominant, but occurs alongside a smaller population of cylindrical domains located towards the centre of many particles (Fig. 3b). In many cases the variability of the lamellar domain spacing as measured from the TEM images was small, and an average domain spacing of ~40 nm (SD = 5 nm) was obtained from 50 measurements. This value corresponds with an expected primary scattering peak position at $q$ = 0.156 $nm^{-1}$ that closely matches the higher $q$ portion of the broad $q^*$ scattering reflection in the SAXS profiles recorded for this sample prior to terminating the reaction (Fig. 3a, $d$ = 40 nm peak), suggesting that this reflection corresponds to the formation of the lamellar morphology. There are also many lamellar regions within these particles that appear to be trapped in an incomplete transition state from the hexagonal cylinder morphology, as identified by their wavy edges, irregular appearance and larger domain spacing values that we partially attribute to the broadening of the lamellar $q^*$ peak to lower values of $q$ (Fig. 3b, $d$ = 49 nm peak).

By contrast, the regions of the particle interiors that possess a hexagonal cylinder morphology show a much broader range of domain sizes that are more difficult to accurately measure from the TEM images because of uneven stretching that occurs during the transition to a lamellar morphology. In spite of this, we estimate an average cylinder-to-cylinder distance of ~50 nm for the domains from 50 measurements, and also attribute the consistent broadening of the primary SAXS scattering peak to lower $q$ values to their presence. Taking the midpoint of this broad peak as the primary $q^*$ scattering reflection also enables the higher order reflection that forms towards the end of the reaction at higher $q$ to be assigned as the expected $3q^*$ reflection for a lamellar morphology (Fig. 3a, $3q^*$ peak). This is further evidence that the lamellar phase forms during the reaction and gradually becomes more prevalent. Such a transition is also anticipated based on the stability window for the lamellar phase in the classical diblock copolymer phase diagram and the $f_{PMMA}$ value of the final product.[2] However, because of a lack of higher order scattering reflections in this sample during the earlier stages of the reaction, the exact sequence of transitions that eventually culminate in the formation of the lamellar morphology could not be identified from these data alone.

### Offline evaluation of morphology evolution for PMMA(25)-PS(50)

To further elucidate the complex phase behaviour during the polymerisation and to estimate a time frame for when the spherical to lamellar phase transition (*via* hexagonal cylinders) occurs, additional TEM images and single shot SAXS data were acquired from the polymer aliquots collected during the offline kinetics evaluation of this reaction (Fig. 4). After reacting for 21 hours an internal morphology of spheres is present throughout the entirety of each particle. By 37 hours the lamellar phase becomes apparent around the edges of some particles alongside the majority spherical phase, and there are also areas within certain particles where arrays of more ordered circular domains indicative of a hexagonally packed cylinder morphology are present.

At 53 hours the prevalence of the spherical phase has declined dramatically, whereas the hexagonally packed cylinder and lamellar morphologies have become abundant to the point where both morphologies are present in roughly equal proportions within the microparticles (see ESI Fig. S13† for a higher magnification TEM image). These observations are qualitatively comparable to those for the microparticles collected at both the 60 hours kinetic time point and from the X-ray autoclave after polymerising for 64 hours during *in situ* SAXS monitoring. This further highlights the very gradual and somewhat sporadic nature of the transitions through phase space for this system and also validates the expected gradual transition of the samples away from the spherical phase and into the morphologies expected for a more symmetrical block copolymer system.[2] To probe the morphology transitions at even higher conversion values than possible at the synchrotron due to time limitations, the kinetics experiment was continued for a further 24 hours beyond the 60 hours time point to gain further insight of the morphological transitions at very high conversion. The final TEM images taken of the product collected after depressurising the autoclave indicated an even higher proportion of particles with a pure lamellar morphology, as expected for this reaction based on the final morphology analysis from previous reports on PMMA-*b*-PS block copolymer microparticles of similar $f_{PMMA}$ values.[34]

Together these data demonstrate that the hexagonal cylinder morphology is a distinct intermediate stage formed during the transition to a lamellar morphology, but that the specific scattering reflection is obscured in the *in situ* SAXS profiles. Its

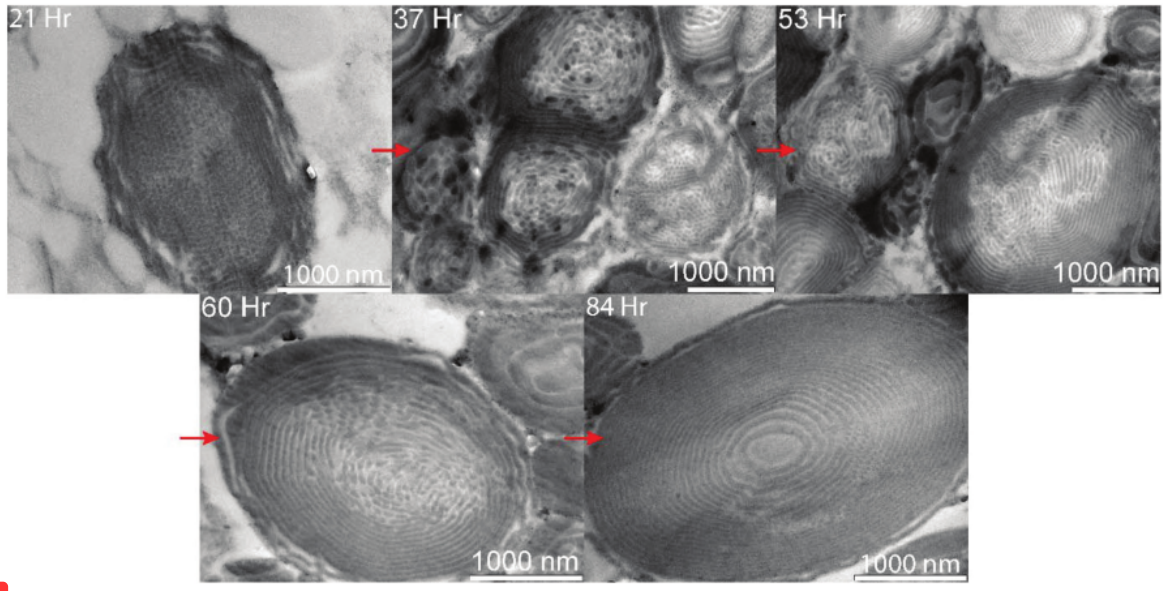


Fig. 4 TEM images of representative cross-sectioned PMMA-*b*-PS particles taken from the kinetic aliquots of the offline chain extension of PMMA(25) with PS(50) at time points of 21, 37, 53, 60 and 84 hours.

appearance within certain particles as elongated and partially fused cylinders also match those described previously by Sakurai *et al.*[65] when a polystyrene-*b*-polybutadiene-*b*-polystyrene (PS-*b*-PB-*b*-PS) block copolymer was thermally induced to undergo a transition from cylinders to lamellae. This occurred through a process in which neighbouring cylinders gradually approached each other before zipping into uninterrupted lamellae.[65] A similar mechanism has also been reported during the transition from high to low order structures in a polystyrene-*b*-polyethylene-*co*-polybutylene-*b*-polystyrene (PS-*b*-PE-*co*-PB-*b*-PS) block copolymer.[66] In this case the cylindrical structure breaks up and forms rippled cylinders as an intermediate prior to transforming into a spherical structure in a selective solvent, which accurately describes the reverse of the transitions observed here. It can therefore be concluded that this spherical to lamellar transition *via* the intermediate hexagonal cylinder morphology initially begins at some point during the 16 hours window between 21–37 hours, corresponding with a PS molecular weight range between ~15–27 kDa based on the kinetics monitoring data (ESI Fig. S6†). These results also suggest that the same transition is likely to have occurred during the early stages of the PMMA(31)-PS(25) polymerisation, immediately after phase separation but prior to formation of the higher order peaks characteristic of a the hexagonal cylinder morphology. For PMMA(31)-PS(25) this occurs after approximately 35 hours of polymerisation and a PS molecular weight of ~15 kDa, suggesting further agreement between the morphology transitions of the two reactions that is obscured in the SAXS data alone due to the lack of higher order scattering information owing to the domain size variation within the microparticles.

### Control polymerisations testing the limits of block copolymer self-organisation in $scCO_2$: synthesis of PMMA(58)-PS(12) and PMMA(54)-PMMA(44) monitored *via in situ* SAXS

As expected, the $q$ ($nm^{-1}$) *versus* $I(q)$ *versus* time plots obtained during the synthesis of the second blocks for PMMA(58)-PS(12) and PMMA(54)-PMMA(44) are both initially featureless (Fig. 5a and ESI Fig. S14,† respectively). This remains the case for the entirety of the PMMA(54)-PMMA(44) polymerisation, indicating that no phase separation occurs during the polymerisation of the second block, and was subsequently corroborated *via* the TEM images taken of the sample post-polymerisation (ESI Fig. S14b†). On the other hand, a single broad scattering peak develops at 0.136 $nm^{-1}$ quite late into the polymerisation of PMMA(58)-PS(12) at approximately 65 hours (see also ESI Fig. S15† for the corresponding 2-dimensional plot of the SAXS profiles at 10 hours intervals). In conjunction with the corresponding TEM images of the final product (Fig. 5b), which lack any evidence of internal phase separated structures, this was assigned as the correlation hole scattering peak indicative of the disordered phase. We attribute the lack of order in this sample to its high degree of block asymmetry ($f_{PMMA}$ = 0.81), positioning it towards the edges of the phase diagram where the formation of ordered structures becomes thermodynamically unfavourable.[2]

### Empirical phase diagram of PMMA-*b*-PS derived from *in situ* SAXS measurements

Block copolymer phase diagrams are powerful tools for researchers needing to target specific morphologies for a system in order to meet an application need. Although both

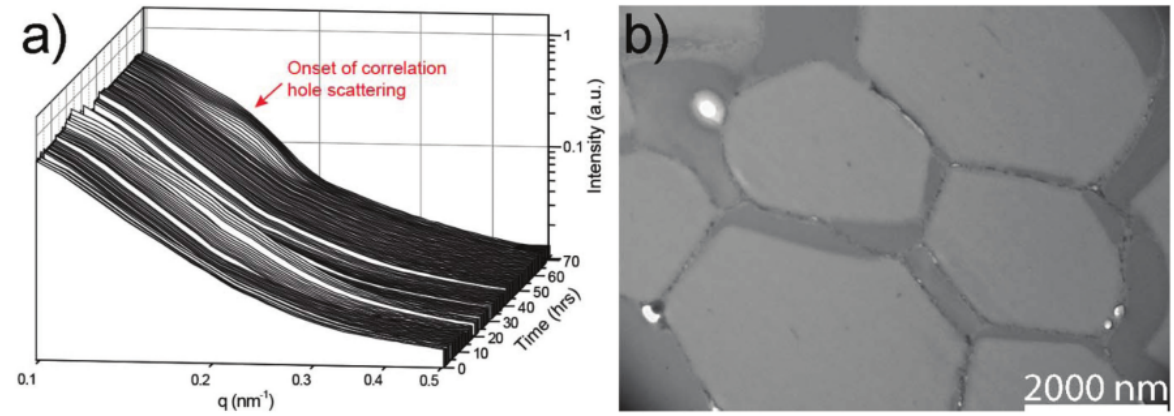


**Fig. 5** (a) Time-resolved *in situ* SAXS data recorded during the chain extension of PMMA(58) to form PMMA(58)-PS(12) *via* dispersion polymerisation in $scCO_2$. The time between the individual profiles included is approximately 30 minutes. (b) TEM images taken of the final product.

theoretically and experimentally derived phase diagrams have been extensively studied and mapped out for neat diblock copolymer systems in the bulk and thin film states, their applicability to ternary systems that contain additives or dopants is often limited.[2,5,12] This is because the additives almost always exhibit preferential affinity for one block, leading to uneven swelling and significantly more complex system thermodynamics. As a result, phase diagrams of such systems must be plotted manually using empirical data taken from static samples, which is a time consuming and experimentally tedious task.[34,58,67]

Previously, Jennings *et al.* have used this approach to plot initial phase diagrams from several static samples of two block copolymer systems, PMMA-*b*-PS and PMMA-*b*-poly(benzyl methacrylate), synthesised *via* one-pot RAFT dispersion polymerisation in $scCO_2$.[34] Although comprised of only a limited number of data points, the diagrams were a more quantitative representation of previous findings that $scCO_2$ preferentially swells methacrylate based polymers over those comprised of styrene units.[36,60] As a consequence, PMMA-*b*-PS block copolymers synthesised in $scCO_2$ demonstrate markedly different morphologies when compared with those in the melt state (see Fig. 6 for the reproduced data). These morphologies are preserved upon venting the $CO_2$ because the block copolymers rapidly revert to a glassy, immobile state at the synthesis temperature (65 °C). For example, at $\chi N$ and $f_{PMMA}$ values of ~30 and ~0.5, respectively, a lamellar morphology is anticipated for a neat diblock copolymer,[2] however, a spherical morphology was observed in an equivalent PMMA-*b*-PS block copolymer synthesised in $scCO_2$.[34]

The rich morphology data that are recorded during a RAFT dispersion polymerisation monitored *in situ* using SAXS are therefore a convenient method for plotting highly accurate empirical phase diagrams from a much smaller subset of polymerisation reactions, when combined with kinetically monitored sample characteristic data. The resulting diagram was plotted using the data points taken from each of the three

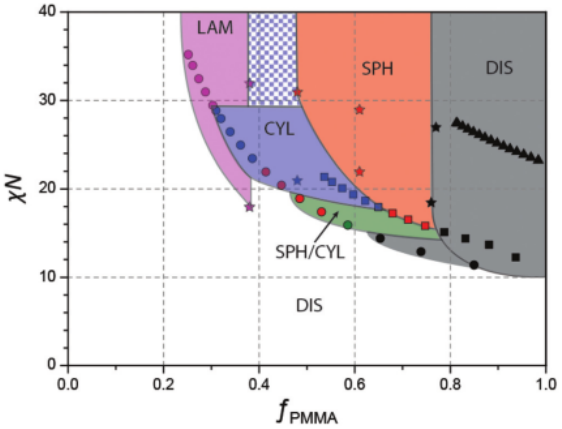


**Fig. 6** Empirical phase diagram for PMMA-*b*-PS in $scCO_2$ derived from the SAXS and kinetics data for PMMA(31)-PS(25) (squares), PMMA(25)-PS(50) (circles) and PMMA(58)-PS(12) (triangles). The data points represented by stars are taken from a previous report by Jennings *et al.* for the same system in $scCO_2$.[34] Where exact time points for morphology transitions could not be determined the phase boundaries were taken at the midpoint between the available data points. The blue checked region is an assumed stability region for the cylindrical morphology that was not observed in the data available.

block copolymer reactions undertaken here at 10 hours intervals (Fig. 6). The data previously reported by Jennings *et al.* for eight static samples of this block copolymer synthesised in $scCO_2$ are also included for easy comparison.[34] In each case, the molecular weight and composition data from GPC and $^1$H NMR spectroscopy, respectively, were used to calculate values of $N$ and $f_{PMMA}$, while the value of $\chi$ at 65 °C was taken from the literature as 0.0395 [56] ($\chi$ = 0.0411 for data plotted from Jennings et al).[34] For simplicity, the molecular weight growth for the reaction of PMMA(58)-PS(12) reaction was assumed to be linear with time with a slope equal to that for PMMA(31)-PS(25).

Very good agreement between the morphology transitions for the three reactions undertaken here and the previous data was observed, thereby solidifying the validity of this approach as being on par with the more conventional approach. This is in spite of additional variables in the $scCO_2$ system, such as temperature, and more importantly, the presence of unreacted monomer, showing that overall their contributions in these systems are low relative to the effects of the $scCO_2$.

## Conclusions

In conclusion, we have demonstrated that the synthesis of nanostructured block copolymer microparticles *via* RAFT dispersion polymerisation in $scCO_2$ can be decoupled into completely independent steps. This was achieved by exploiting the living chain ends of RAFT synthesised PMMA homopolymers, even after storage for months, and their ability to be quickly redispersed in $scCO_2$ using a small quantity of additional PDMS-MA stabiliser. Using this process a series of three PMMA-*b*-PS block copolymers with varying $f_{PMMA}$ ratios were synthesised and the development of order and subsequent morphology evolution was monitored throughout the polymerisation *via in situ* SAXS and corroborated using post-mortem TEM imaging. For the polymerisation of PMMA(31)-PS(25) a SAXS pattern consistent with a hexagonal cylinder morphology was gradually formed following phase separation at approximately 16 hours. The characteristic spacing then gradually increased with time in response to the growing PS block until the end of the reaction and no further morphology transitions occurred. TEM imaging confirmed the presence of this morphology and additional SAXS analysis of the final product revealed that the domain size of the sample following depressurisation was almost the same value prior to venting the autoclave at the end of the reaction. This indicates that the increase in domain size of the internal morphology brought about by the swelling effects of $scCO_2$ are mostly retained by the sample upon its removal.

By contrast, the SAXS profiles obtained during the synthesis of PMMA(25)-PS(50) were considerably more complex. Initially a single broad peak was discernible in the SAXS profiles of this sample at 13.5 hours, which from the TEM images taken at a slightly later time was revealed to be due to the initial formation of a spherical morphology. As the polymerisation progressed this SAXS peak became progressively broader and slightly bimodal in appearance as the spheres gradually transitioned into a mixed cylindrical/lamellar phase. To further elucidate the nature and time period of this transition the reaction was repeated in a sampling autoclave and aliquots were taken at various time points for TEM analysis. These images revealed that the transition from spheres begins to occur over a 16 hours window between 21–37 hours *via* a hexagonally packed cylinder morphology intermediate. This is a slow and somewhat sporadic process that remains partially incomplete until the very late stages of the polymerisation ($t$ > 64 hours). Finally, for PMMA(58)-PS(12) a disordered peak appeared late into the polymerisation but no self-organisation occurred due to the highly asymmetric composition of this sample, while for PMMA(54)-PMMA(44) there was no evidence of phase separation.

## Conflicts of interest

There are no conflicts to declare.

## Acknowledgements

SAXS experiments were undertaken at Beamline 26B (DUBBLE) of the European Synchrotron and Radiation Facility (ESRF) in Grenoble, France. We thank the N.W.O for providing the beam time for our experiments. We gratefully acknowledge the University of Nottingham Nanoscale and Microscale Research Centre (NMRC) for access to their instrumentation, in particular Ms Denise McCl[illegible] for assistance with the FEI Tecnai TEM. MA, TMB, GH and SMH are indebted to the very high quality technical and high pressure safety support at the University of Nottingham from Peter Fields, Richard Wilson and Martin Dellar. This research was supported in part under the Leverhulme Grant Award Scheme (RPG-2014-034, for TMB, GH and SMH) as well a UNNES-IDB PhD scholarship for MA.

## References

1 L. Leibler, *Macromolecules*, 1980, **13**, 1602–1617.
2 M. W. Matsen and F. S. Bates, *Macromolecules*, 1996, **29**, 1091–1098.
3 M. W. Matsen and M. Schick, *Phys. Rev. Lett.*, 1994, **72**, 2660–2663.
4 R. A. Segalman, *Mater. Sci. Eng., R*, 2005, **48**, 191–226.
5 A. K. Khandpur, S. Foerster, F. S. Bates, I. W. Hamley, A. J. Ryan, W. Bras, K. Almdal and K. Mortensen, *Macromolecules*, 1995, **28**, 8796–8806.
6 H. Yu, X. Qiu, S. P. Nunes and K.-V. Peinemann, *Nat. Commun.*, 2014, **5**, 4110.
7 D. Mecerreyes, *Prog. Polym. Sci.*, 2011, **36**, 1629–1648.
8 V. F. Scalfani, E. F. Wiesenauer, J. R. Ekblad, J. P. Edwards, D. L. Gin and T. S. Bailey, *Macromolecules*, 2012, **45**, 4262–4276.
9 K.-V. Peinemann, V. Abetz and P. F. W. Simon, *Nat. Mater.*, 2007, **6**, 992–996.
10 Y. Fink, A. M. Urbas, M. G. Bawendi, J. D. Joannopoulos and E. L. Thomas, *J. Lightwave Technol.*, 1999, **17**, 1963–1969.
11 Y. Kang, J. J. Walish, T. Gorishnyy and E. L. Thomas, *Nat. Mater.*, 2007, **6**, 957–960.
12 C. T. Black, R. Ruiz, G. Breyta, J. Y. Cheng, M. E. Colburn, K. W. Guarini, H. C. Kim and Y. Zhang, *IBM J. Res. Dev.*, 2007, **51**, 605–633.
13 J. G. Kennemur, L. Yao, F. S. Bates and M. A. Hillmyer, *Macromolecules*, 2014, **47**, 1411–1418.
14 T. M. Bennett, K. Pei, H.-H. Cheng, K. J. Thurecht, K. S. Jack and I. Blakey, *J. Micro/Nanolithogr., MEMS, MOEMS*, 2014, **13**, 031304.

15 I. Botiz and S. B. Darling, *Mater. Today*, 2010, **13**, 42–51.
16 H.-Y. Hsueh, H.-Y. Chen, M.-S. She, C.-K. Chen, R.-M. Ho, S. Gwo, H. Hasegawa and E. L. Thomas, *Nano Lett.*, 2010, **10**, 4994–5000.
17 M. G. Fischer, X. Hua, B. D. Wilts, I. Gunkel, T. M. Bennett and U. Steiner, *ACS Appl. Mater. Interfaces*, 2017, **9**, 22388–22397.
18 T. M. Bennett, G. He, R. R. Larder, M. G. Fischer, G. A. Rance, M. W. Fay, A. K. Pearce, C. D. J. Parmenter, U. Steiner and S. M. Howdle, *Nano Lett.*, 2018, **18**, 7560–7569.
19 J. Jennings, G. He, S. M. Howdle and P. B. Zetterlund, *Chem. Soc. Rev.*, 2016, **45**, 5055–5084.
20 B. H. Jones and T. P. Lodge, *ACS Nano*, 2011, **5**, 8914–8927.
21 H. Sai, K. W. Tan, K. Hur, E. Asenath-Smith, R. Hovden, Y. Jiang, M. Riccio, D. A. Muller, V. Elser, L. A. Estroff, S. M. Gruner and U. Wiesner, *Science*, 2013, **341**, 530–534.
22 T. Higuchi, A. Tajima, K. Motoyoshi, H. Yabu and M. Shimomura, *Angew. Chem., Int. Ed.*, 2008, **47**, 8044–8046.
23 T. Higuchi, A. Tajima, H. Yabu and M. Shimomura, *Soft Matter*, 2008, **4**, 1302–1305.
24 L. Li, K. Matsunaga, J. Zhu, T. Higuchi, H. Yabu, M. Shimomura, H. Jinnai, R. C. Hayward and T. P. Russell, *Macromolecules*, 2010, **43**, 7807–7812.
25 S.-J. Jeon, G.-R. Yi, C. M. Koo and S.-M. Yang, *Macromolecules*, 2007, **40**, 8430–8439.
26 S.-J. Jeon, G.-R. Yi and S.-M. Yang, *Adv. Mater.*, 2008, **20**, 4103–4108.
27 K. H. Ku, H. Yang, J. M. Shin and B. J. Kim, *J. Polym. Sci., Part A: Polym. Chem.*, 2015, **53**, 188–192.
28 Z. Lu, G. Liu and F. Liu, *Macromolecules*, 2001, **34**, 8814–8817.
29 A. Nykänen, A. Rahikkala, S.-P. Hirvonen, V. Aseyev, H. Tenhu, R. Mezzenga, J. Raula, E. Kauppinen and J. Ruokolainen, *Macromolecules*, 2012, **45**, 8401–8411.
30 D. J. Keddie, *Chem. Soc. Rev.*, 2014, **43**, 496–505.
31 B. Charleux, G. Delaittre, J. Rieger and F. D'Agosto, *Macromolecules*, 2012, **45**, 6753–6765.
32 N. J. Warren and S. P. Armes, *J. Am. Chem. Soc.*, 2014, **136**, 10174–10185.
33 M. J. Derry, L. A. Fielding and S. P. Armes, *Prog. Polym. Sci.*, 2016, **52**, 1–18.
34 J. Jennings, S. P. Bassett, D. Hermida-Merino, G. Portale, W. Bras, L. Knight, J. J. Titman, T. Higuchi, H. Jinnai and S. M. Howdle, *Polym. Chem.*, 2016, **7**, 905–916.
35 J. Jennings, M. Beija, J. T. Kennon, H. Willcock, R. K. O'Reilly, S. Rimmer and S. M. Howdle, *Macromolecules*, 2013, **46**, 6843–6851.
36 J. Jennings, M. Beija, A. P. Richez, S. D. Cooper, P. E. Mignot, K. J. Thurecht, K. S. Jack and S. M. Howdle, *J. Am. Chem. Soc.*, 2012, **134**, 4772–4781.
37 G. He, T. M. Bennett, M. Alauhdin, M. W. Fay, X. Liu, S. T. Schwab, C.-g. Sun and S. M. Howdle, *Polym. Chem.*, 2018, **9**, 3808–3819.
38 T. D. McAllister, L. D. Farrand and S. M. Howdle, *Macromol. Chem. Phys.*, 2016, **217**, 2294–2301.
39 A. I. Cooper, *J. Mater. Chem.*, 2000, **10**, 207–234.
40 C. Boyère, C. Jérôme and A. Debuigne, *Eur. Polym. J.*, 2014, **61**, 45–63.
41 S. Curia, D. S. A. De Focatiis and S. M. Howdle, *Polymer*, 2015, **69**, 17–24.
42 S. Curia, A. F. Barclay, S. Torron, M. Johansson and S. M. Howdle, *Philos. Trans. R. Soc., A*, 2015, 373.
43 I. Kikic, *J. Supercrit. Fluids*, 2009, **47**, 458–465.
44 E. Girard, T. Tassaing, J.-D. Marty and M. Destarac, *Chem. Rev.*, 2016, **116**, 4125–4169.
45 S. Hilic, S. A. E. Boyer, A. A. H. Pádua and J.-P. E. Grolier, *J. Polym. Sci., Part B: Polym. Phys.*, 2001, **39**, 2063–2070.
46 R. Li, Z. Zhang and T. Fang, *J. Supercrit. Fluids*, 2016, **110**, 110–116.
47 B. Chu and B. S. Hsiao, *Chem. Rev.*, 2001, **101**, 1727–1762.
48 M. J. Elwell, S. Mortimer and A. J. Ryan, *Macromolecules*, 1994, **27**, 5428–5439.
49 H. S. Lee, S. R. Yoo and S. W. Seo, *Fibers Polym.*, 2001, **2**, 98.
50 M. J. Derry, L. A. Fielding, N. J. Warren, C. J. Mable, A. J. Smith, O. O. Mykhaylyk and S. P. Armes, *Chem. Sci.*, 2016, **7**, 5078–5090.
51 D. Hermida-Merino, G. Portale, P. Fields, R. Wilson, S. P. Bassett, J. Jennings, M. Dellar, C. Gommes, S. M. Howdle, B. C. M. Vrolijk and W. Bras, *Rev. Sci. Instrum.*, 2014, **85**, 093905.
52 J. T. Lai, D. Filla and R. Shea, *Macromolecules*, 2002, **35**, 6754–6756.
53 A. M. Gregory, K. J. Thurecht and S. M. Howdle, *Macromolecules*, 2008, **41**, 1215–1222.
54 W. Bras, I. P. Dolbnya, D. Detollenaere, R. van Tol, M. Malfois, G. N. Greaves, A. J. Ryan and E. Heeley, *J. Appl. Crystallogr.*, 2003, **36**, 791–794.
55 J. Brandrup, E. H. Immergut and E. A. Grulke, *Polymer Handbook*, Wiley, 4th edn, 1999.
56 T. P. Russell, R. P. Hjelm and P. A. Seeger, *Macromolecules*, 1990, **23**, 890–893.
57 H. Ahn, D. Y. Ryu, Y. Kim, K. W. Kwon, J. Lee and J. Cho, *Macromolecules*, 2009, **42**, 7897–7902.
58 T. M. Bennett, K. S. Jack, K. J. Thurecht and I. Blakey, *Macromolecules*, 2016, **49**, 205–214.
59 M. L. Hoarfrost and R. A. Segalman, *ACS Macro Lett.*, 2012, **1**, 937–943.
60 Y. Zhang, K. K. Gangwani and R. M. Lemert, *J. Supercrit. Fluids*, 1997, **11**, 115–134.
61 M. Zhong and K. Matyjaszewski, *Macromolecules*, 2011, **44**, 2668–2677.
62 T. Tanaka, M. Okayama, Y. Kitayama, Y. Kagawa and M. Okubo, *Langmuir*, 2010, **26**, 7843–7847.
63 T. Rieker, A. Hanprasopwattana, A. Datye and P. Hubbard, *Langmuir*, 1999, **15**, 638–641.
64 F. S. Bates, *Macromolecules*, 1985, **18**, 525–528.
65 S. Sakurai, T. Momii, K. Taie, M. Shibayama, S. Nomura and T. Hashimoto, *Macromolecules*, 1993, **26**, 485–491.
66 M. Li, Y. Liu, H. Nie, R. Bansil and M. Steinhart, *Macromolecules*, 2007, **40**, 9491–9502.
67 T. P. Lodge, B. Pudil and K. J. Hanley, *Macromolecules*, 2002, **35**, 4707–4717.

# Monitoring morphology evolution within block copolymer microparticles during dispersion polymerisation in supercritical carbon dioxide: a high pressure SAXS study

ORIGINALITY REPORT

| 12% | % | 12% | % |
|---|---|---|---|
| SIMILARITY INDEX | INTERNET SOURCES | PUBLICATIONS | STUDENT PAPERS |

PRIMARY SOURCES

| | | |
|---|---|---|
| 1 | J. Jennings, S. P. Bassett, D. Hermida-Merino, G. Portale et al. " How does dense phase CO influence the phase behaviour of block copolymers synthesised by dispersion polymerisation? ", Polymer Chemistry, 2016<br>Publication | 2% |
| 2 | Guping He, Thomas M. Bennett, Kartini Alias, Long Jiang, Simon T. Schwab, Mohammad Alauhdin, Steven M. Howdle. " crosslinking of nanostructured block copolymer microparticles in supercritical carbon dioxide ", Polymer Chemistry, 2019<br>Publication | 2% |
| 3 | Jennings, James, Mariana Beija, Alexandre P. Richez, Samuel D. Cooper, Paul E. Mignot, Kristofer J. Thurecht, Kevin S. Jack, and Steven M. Howdle. "One-Pot Synthesis of Block Copolymers in Supercritical Carbon Dioxide: A Simple Versatile Route to Nanostructured | 1% |

Microparticles", Journal of the American Chemical Society, 2012.
Publication

---

4 Jennings, James, Mariana Beija, Jeremy T. Kennon, Helen Willcock, Rachel K. O'Reilly, Stephen Rimmer, and Steven M. Howdle. "Advantages of Block Copolymer Synthesis by RAFT-Controlled Dispersion Polymerization in Supercritical Carbon Dioxide", Macromolecules, 2013. 1 %
Publication

---

5 Ryan R. Larder, Thomas M. Bennett, L. Scott Blankenship, Jesum A. Fernandes et al. " Porous hollow TiO microparticles for photocatalysis: exploiting novel ABC triblock terpolymer templates synthesised in supercritical CO ", Polymer Chemistry, 2021 1 %
Publication

---

6 Brad H. Jones, Timothy P. Lodge. "Hierarchically Structured Materials from Block Polymer Confinement within Bicontinuous Microemulsion-Derived Nanoporous Polyethylene", ACS Nano, 2011 1 %
Publication

---

7 Natasha A. Birkin, Oliver J. Wildig, Steven M. Howdle. "Effects of poly(vinyl pivalate)-based stabiliser architecture on CO2-solubility and stabilising ability in dispersion polymerisation 1 %

of N-vinyl pyrrolidone", Polymer Chemistry, 2013
Publication

---

8 Daniel Hermida-Merino, Giuseppe Portale, Peter Fields, Richard Wilson et al. " A high pressure cell for supercritical CO on-line chemical reactions studied with x-ray techniques ", Review of Scientific Instruments, 2014 <1%
Publication

---

9 Thomas M. Bennett, Julien Portal, Valérie Jeanne-Rose, Simon Taupin, Alexander Ilchev, Derek J. Irvine, Steven M. Howdle. "Synthesis of model terpene-derived copolymers in supercritical carbon dioxide for cosmetic applications", European Polymer Journal, 2021 <1%
Publication

---

10 J. Jennings, G. He, S. M. Howdle, P. B. Zetterlund. "Block copolymer synthesis by controlled/living radical polymerisation in heterogeneous systems", Chemical Society Reviews, 2016 <1%
Publication

---

11 Matthew J. Derry, Lee A. Fielding, Nicholas J. Warren, Charlotte J. Mable et al. " small-angle X-ray scattering studies of sterically-stabilized diblock copolymer nanoparticles formed <1%

during polymerization-induced self-assembly in non-polar media ", Chem. Sci., 2016
Publication

---

12 MacDonald, J. P., M. P. Parker, B. W. Greenland, D. Hermida-Merino, I. W. Hamley, and M. P. Shaver. "Tuning thermal properties and microphase separation in aliphatic polyester ABA copolymers", Polymer Chemistry, 2014.
Publication

<1 %

---

13 Martin Faber, Anton H. Hofman, Evgeny Polushkin, Gert Alberda van Ekenstein et al. "Hierarchical Self-Assembly in Supramolecular Double-Comb Diblock Copolymer Complexes", Macromolecules, 2013
Publication

<1 %

---

14 Ana A. C. Pacheco, Arnaldo F. da Silva Filho, Kristoffer Kortsen, Magnus W. D. Hanson-Heine et al. " Influence of structure and solubility of chain transfer agents on the RAFT control of dispersion polymerisation in scCO ", Chemical Science, 2021
Publication

<1 %

---

15 Jin-Seong Kim, Jee-Eun Choi, Hyeonjung Park, Youngkwon Kim, Hyeong Jun Kim, Junghun Han, Jae Man Shin, Bumjoon J. Kim. " Synthesis and crystallization behavior of regioregular- -regiorandom poly(3-

<1 %

hexylthiophene) copolymers ", Polymer Chemistry, 2019
Publication

---

16 Van Assche, Guy, Bruno Van Mele, Ting Li, and Erik Nies. "Adjacent UCST Phase Behavior in Aqueous Solutions of Poly(vinyl methyl ether): Detection of a Narrow Low Temperature UCST in the Lower Concentration Range", Macromolecules, 2011. <1 %
Publication

---

17 Ryan R Larder, Thomas M Bennett, Leo S Blankenship, Jesum Alves Fernandes et al. "Porous Hollow TiO2 Microparticles for Photocatalysis: Exploiting Novel ABC Triblock Terpolymer Templates Synthesised in Supercritical CO2", Polymer Chemistry, 2021 <1 %
Publication

---

18 Simon P. Bassett, Natasha A. Birkin, James Jennings, Emma Chapman, Rachel K. O'Reilly, Steven M. Howdle, Helen Willcock. "One-pot synthesis of micron-sized polybetaine particles; innovative use of supercritical carbon dioxide", Polym. Chem., 2017 <1 %
Publication

---

19 Farrell, R.A.. "Self-assembled templates for the generation of arrays of 1-dimensional nanostructures: From molecules to devices", <1 %

Journal of Colloid And Interface Science, 20100915
Publication

20 J. Puig, M. Ceolín, R. J. J. Williams, W. F. Schroeder, I. A. Zucchi. "Controlling the generation of bilayer and multilayer vesicles in block copolymer/epoxy blends by a slow photopolymerization process", Soft Matter, 2017
Publication

<1 %

| | | | |
|---|---|---|---|
| Exclude quotes | On | Exclude matches | < 20 words |
| Exclude bibliography | On | | |